Iranian Journal of Basic Medical Sciences
ijbms.mums.ac.ir

Enhanced bone regeneration and cellular protection from oxidative stress using a vitamin C-based scaffold

Paulra Sharmila [1], Sundaram Ramkumar [2], Sivagami Sivagami [3], Sivathanu Suja [4], Tamilarasan Ramalingam [5]*, Pandurengan Kamalarajan [6], Dharman Govindaraj [7], Kalaiyarasi Jayaprakash [8]

[1] Department of Physics, Prince Shri Venkateshwara Padmavathy Engineering college, Ponmar, Chennai, Tamil Nadu, India -600 127
[2] Department of Electronics and Communication Engineering, Sri Eshwar College of Engineering, Coimbatore, Tamil Nadu, India -641202
[3] Department of Chemistry, New Prince Shri Bhavani College of Engineering and Technology, Chennai, Tamil Nadu, India- 600073
[4] Department of Chemistry, S. A. Engineering College, Thiruverkadu, Chennai, Tamil Nadu, India-600 077
[5] Department of Chemistry, Rajalakshmi Institute of Technology, Kuthambakkam, Chembarambakkam, Tamil Nadu, India -600124
[6] Department of Chemistry, R.M.D. Engineering College, Tiruvallur, Tamil Nadu, India - 601 206
[7] Centre for Nanobiomedicine, Sciliv Pvt Ltd, Dharmapuri, Tamilnadu, India-636701
[8] Center for Bioanalytical research, Sciliv Pvt Ltd, Dharmapuri, Tamilnadu, India-636701

ARTICLE INFO

Article type:
Original

Article history:
Received: Aug 21, 2025
Accepted: Oct 19, 2025

Keywords:
Biomineralization
Cytocompatibility
Osseointegration
Osteoconductive
Osteoinductive

ABSTRACT

Objective(s): To fabricate and investigate a novel VitC@HAP-HYA nanocomposite scaffold that combines the osteoconductive attributes of hydroxyapatite (HAP), the extracellular matrix-replicating properties of hyaluronic acid (HYA), and the osteoinductive/antioxidant effects of Vitamin C (VitC) for enhanced bone regeneration.

Materials and Methods: The composite was developed using an in-situ precipitation method. Physicochemical characterisation (FT-IR, XRD, and HR-TEM) was used to validate the composition, crystallinity, and shape. The examination of Simulated Body Fluid (SBF) evaluated bioactivity. The biological assessments used the MC3T3-E1 osteoblast-like cell line, including MTT and AO/PI tests for biocompatibility, DAPI labelling for cell colonization, Alkaline Phosphatase (ALP) activity to assess early osteogenic differentiation, and Alizarin Red S (ARS) staining for biomineralization analysis. Monitoring of intracellular Reactive Oxygen Species (ROS) evaluated its cytoprotective efficacy against oxidative stress.

Results: FT-IR and XRD analyses confirmed the effective integration of amorphous VitC and HYA into HAP, yielding a stable 120 nm nanocomposite. The SBF study demonstrated fast production of a calcium phosphate layer, indicating elevated bioactivity. In cell culture, VitC@HAP-HYA demonstrated enhanced cell survival and colonization, as well as strong biocompatibility. It markedly improved early-stage osteogenic commitment and late-stage biomineralization compared with HAP and HAP-HYA controls. Moreover, the composite exhibited enhanced cytoprotective properties by inhibiting intracellular ROS in H2O2-treated cells.

Conclusion: The VitC@HAP-HYA composite effectively combines multifunctional qualities, demonstrating superior bioactivity, increased osteogenic potential, and vital cytoprotective features. These results robustly endorse its potential as a sophisticated framework for bone tissue engineering, including applications such as anti-cancer bone excision repair.

▶Please cite this article as
Sharmila P, Ramkumar S, Sivagami S, Suja S, Ramalingam T,Kamalarajan P, Govindaraj D, Jayaprakash K. Enhanced bone regeneration and cellular protection from oxidative stress using a vitamin C-based scaffold. Iran J Basic Med Sci 2026; 29:

Introduction

Bone tissue is a dynamic and intricate structure with exceptional regenerating capabilities. In instances of critical-sized defects caused by trauma, tumor removal, or congenital malformations, the inherent healing capacity is inadequate, requiring surgical intervention and the application of bone transplants (1). Bone tissue engineering (BTE) has emerged as a promising multidisciplinary field dedicated to the creation of biomimetic scaffolds that integrate suitable cells and bioactive molecules to proficiently repair or replace injured bone tissue (2).

The constraints of the prevailing clinical gold standard for bone regeneration, namely autografts, have catalyzed extensive research into alternative methodologies. Although autografts are esteemed for their possession of the three essential properties—osteoconductive, osteoinductive, and osteogenic—as well as their non-immunogenicity, their clinical application is significantly constrained by substantial limitations (3, 4). Key concerns include donor site morbidity, including persistent pain or nerve damage at the bone harvest location, limited availability for extensive or numerous abnormalities, and the intrinsic risk of infection and extended operational duration (4, 5). These issues need the creation of synthetic bone replacements that may successfully mimic the advantageous features of autografts while avoiding their associated risks and resource limitations. Allografts and xenografts provide alternative solutions but carry the risks of disease transmission

***Corresponding author:** Tamilarasan Ramalingam. Department of Chemistry, Rajalakshmi Institute of Technology, Kuthambakkam, Chembarambakkam, Tamil Nadu, India -600124. Email: ramasusitamil@gmail.com

and immunological rejection (6, 7). Thus, the prevailing direction in BTE focuses on developing synthetic and composite biomaterials that address these constraints by mimicking the architecture and biological functions of natural bone (8, 9).

An optimal bone scaffold requires several factors: it must be biocompatible, osteoconductive, possibly osteoinductive, biodegradable at a controlled rate, and mechanically robust (10). Many available biomaterials have crucial drawbacks. Pure polymers often exhibit insufficient mechanical strength or bioactivity compared to natural bone, while several ceramics may be too brittle or degrade too slowly (11, 12). Bridging this gap necessitates the creation of hybrid nanocomposites that integrate the advantages of many material categories.

Hydroxyapatite (HAP) is the principal inorganic element of natural bone and dental structures. Its chemical composition, non-toxicity, and remarkable osteoconductive characteristics make it one of the most prevalent bioceramics in regenerative medicine (13, 14). Nano-sized hydroxyapatite (n-HAP) significantly increases surface area and dissolution kinetics, closely resembling the mineral phase of natural bone and facilitating cellular interactions. Nonetheless, pure HAP scaffolds often exhibit insufficient mechanical flexibility and inadequate signals for cell adhesion and proliferation owing to their rigid, entirely inorganic composition (15, 16).

Hyaluronic Acid (HYA), a key element of the extracellular matrix (ECM) of connective tissues, is an anionic, non-sulphated glycosaminoglycan (17). HYA uses in BTE are extensive: it exhibits great biocompatibility, non immunogenicity, and is essential in modulating cell adhesion, migration, and differentiation (18, 19). Moreover, its capacity to generate hydrogels and its structural resemblance to the organic ECM component provide a conducive environment for cellular activity, notably improving cell adhesion and nutrient transfer, which are essential for tissue development. The synergistic incorporation of HAP and HYA (HAP-HYA) aims to produce a composite that preserves the osteoconductivity of the ceramic component while providing the biological encouragement and adaptability of the polymeric component.

Notwithstanding enhanced structure and biocompatibility, several HAP-polymer composites continue to need an external stimulation for effective bone regeneration (20, 21). VitC (ascorbic acid) is a potent water-soluble antioxidant and a crucial cofactor for several biological processes. Its implications for bone health are significant, principally due to its function as an essential cofactor for prolyl and lysyl hydroxylase enzymes, which are vital for the post-translational modification and cross-linking of collagen, the principal organic component of bone (22, 23). Furthermore, VitC directly induces osteogenic differentiation by enhancing the expression of key markers, such as Alkaline Phosphatase, and boosting biomineralization. The integration of VitC into the HAP-HYA matrix, resulting in a VitC-loaded HAP-HYA composite, constitutes an approach for developing a truly osteoinductive biomaterial that may actively facilitate the bone regeneration process *in situ*.

The distinct components (HAP, HAP-HYA, and VitC@HAP-HYA) have been examined; however, the effective amalgamation of all three into a stable, functional nanocomposite with improved osteogenic potential is a considerable hurdle. In reviewing previously published articles, numerous studies have concentrated on binary systems (HAP-VitC or HAP-HYA), while fewer have investigated the synergistic triad, particularly regarding its influence on both early (ALP activity, cell proliferation) and late-stage (biomineralization) osteogenic markers, as well as essential cytoprotective effects (24, 25). Many recent publications suggest that VitC has a beneficial effect on HAP scaffolds; however, they often lack the ECM support provided by HYA (26, 27). In contrast, HAP-HYA systems may exhibit favorable mechanical and adhesive properties but lack the prolonged osteoinductive effect of a bioactive substance such as VitC (28, 29).

To address this requirement, the VitC@HAP-HYA nanocomposite was efficiently produced and thoroughly described in this study. Anticipate that the chemical interactions of this trio will provide a stable nanocomposite exhibiting remarkable biological activity. Before using HR-TEM to analyze morphology and particle-size evolution, FT-IR and XRD were used to confirm successful conjugation and the crystalline structure. The biological performance was comprehensively evaluated, including osteogenic differentiation (ALP activity, biomineralization via ARS staining), biocompatibility (MTT, Live/Dead, Colony formation), in vitro bioactivity (SBF analysis), and the essential role of VitC in cytoprotection against oxidative stress. The aggregated findings provide compelling evidence that the VitC@HAP-HYA nanocomposite serves as a highly promising scaffold, integrating osteoconductivity, osteoinductivity, and ECM mimicry to enhance bone tissue regeneration.

Materials and Methods

Synthesis of vitC@HAP-HYA composites

All chemicals were purchased from Sigma Aldrich in India and were of analytical quality, requiring no additional processing. The VitC@HAP-HYA composite was created using the in-situ precipitation technique. Initially, 2 g of HYA and 2 g of L-ascorbic acid (VitC) were solubilized in 40 ml of deionized water to create the VitC-HYA solution. The solution was amalgamated with 20 mL of 1 M Ca $(NO_3)_2$ and stirred until a homogeneous mixture was obtained. Subsequently, 20 mL of a 0.6 M H_3PO_4 solution was gradually added to the Ca $(NO_3)_2$-VitC-HYA solution. The p^H was adjusted to a basic range by dropwise addition of 50 ml of include 0.1 M NaOH solution. The mixture was homogenized for 20 min at room temperature with a probe sonicator. The resultant solution was further centrifuged at 5000 rpm, and the obtained precipitate (VitC@HAP-HYA composite) was subjected to freeze-drying. For comparison analysis, HAP-HYA and pure HAP were synthesized using the same technique, excluding VitC for HAP-HYA and both VitC and HYA for pure HAP.

Characterization of vitC@HAP-HYA

Fourier Transform Infrared Spectroscopy (FT-IR) was conducted to analyze the formulated nanocomposites (HAP, HYA, HAP-HYA, VitC@HAP-HYA). Approximately 0.1 g of each powdered sample was meticulously pulverized with 0.5 g of spectroscopic-grade KBr. The hydraulic press was used to compress the slurry into a clear disk. FT-IR spectra were obtained within the range of 400-4000 cm^{-1} using an Agilent

Cary 630 FT-IR and 4300 Handheld FT-IR spectrometers. XRD studies were performed to examine the crystallinity and phase composition of the produced nanoparticles. The investigation used (Malvern Panalytical: Empyrean, Aeris) with a monochromated Cu Kα source functioning at 30 kV and 30 mA. The samples were analyzed in step-scan mode over a 2θ range, with a step size of 0.02 °/min and a scan rate of 0.02 °/min. To prepare the HR-TEM sample, the nanocomposite was dissolved in ethanol and then sonicated for five minutes to ensure homogeneity. Before examination, a suspension droplet was carefully placed on a 300-mesh copper carbon grid and air-dried.

In vitro mineralization

The preparation of the *in vitro* mineralization simulated body fluid (SBF) solution was conducted according to previously reported methods (30). To examine apatite production and the bioactivity of the samples, the sterilized composite samples were immersed in SBF. Each sample was placed in 25 ml of SBF and incubated under static conditions in a controlled environment maintained at 37 ˚C. To study the mineralization that occurred over an extended period, a 14-day incubation period was used. Every two days, the SBF medium was entirely swapped out in order to maintain a constant and favorable supersaturation condition that was favourable to the deposition of apatite. After the conclusion of the incubation period, the mineralized hydrogel composites were carefully extracted and then rinsed three times with ultra-pure water in order to get rid of any remaining components of the SBF and weakly bound surface salts. After that, the samples were freeze-dried in preparation for further analysis that would be performed on them. SEM was used in the analysis of the surface morphology and elemental composition of the deposited mineral layer.

Cell culture maintenance

The murine calvarial osteoblast-like cell line, MC3T3-E1 were obtained from the National Centre for Cell Science (NCCS), Pune, India. Cells were maintained in DMEM/F-12 nutrient mixture supplemented with 10% FBS and 1% penicillin/streptomycin. Cultures were kept in a humidified incubator at 37 ˚C with 5% CO_2.

MC3T3-E1 were inoculated at a density of 2×10^4 in 24-well tissue culture plates. Osteogenic differentiation (OSD) was induced by replacing the growth medium with FBS and antibiotics. HAP, HAP-HYA, and VitC@HAP-HYA were added to the differentiation medium at a final dosage of 15 mg/ml after dilution with DMSO. The control group was served differentiation medium alone. The cells were sustained in a humidified incubator at 37 ˚C with 5% CO_2, and the differentiation medium was replenished every 3 days for 7 days. Morphological alterations were observed using an inverted light microscope.

Alkaline phosphatase (ALP) assay

Bone-specific alkaline phosphatase (ALP) activity was measured in culture supernatants to assess how osteocytes deposit hardened ECM. We got supernatants three, seven, and fourteen days after OSD was started. The manufacturer's instructions were followed to test the ALP levels using a Kit (26). A standard curve was prepared by gradually diluting the provided ALP standards. Samples and standards were placed on an ELISA plate that had already been covered, and the plate was incubated at 37 ˚C for 80 min. After being washed, a biotinylated anti-ALP antibody was added and incubated for 1.2 hours at 37 ˚C. It was then treated with avidin-HRP conjugate for 20 min at the same temperature. The substrate solution was added after extensive washing, and the mixture was incubated at 37 ˚C for 10 min. Eventually, a stock solution was added, and the OD at 450 nm was measured with a microplate reader.

Cell viability analysis

The viability of MC3T3-E1 cells was assessed at 3, 7, and 14 days into 3, 5, and 7 days post-induction of OSD utilizing the standard MTT assay. Before enumeration, the culture medium was removed, and the cells underwent two washes with PBS. Cells were detached through trypsinization and collected by centrifugation at 500 ×g for 5 min. The cell pellets obtained were resuspended in PBS. Viable cell counts were determined using an automatic cell counter (Mindray 96a ELISA reader) by excluding cells that excluded the MTT dye to evaluate viability, as previously outlined (31). Cell morphology and qualitative assessment were conducted utilizing an Olympus CKX53 inverted microscope**.**

OSD staining assay

Matrix mineralization was evaluated by staining cells with Alizarin Red S (ARS) at multiple time points after osteogenic induction. The culture medium was systematically removed and discarded on days 3, 7, and 14 days into 3, 5, and 7 days following the induction of OSD. Before staining, the cells were subjected to two gentle washes with 1× PBS. The cells were fixed for 15 min at room temperature with freshly prepared 3% Paraformaldehyde (PFA). After fixation, the cells underwent two washes with 1× PBS to eliminate residual PFA. The fixed cells were incubated with a working solution of ARS for 15 min at room temperature. The solution employed was 2% ARS in deionized water, with the p^H meticulously adjusted to 4.0-4.5 using 0.1 M NaOH. Non-specifically bound stain was removed by thoroughly washing the cells with distilled water until no discoloration was observed in the wash water. Stained mineralized deposits, appearing as red nodules, were systematically examined and recorded utilizing an Olympus CKX53 inverted microscope (Olympus Corporation, Tokyo, Japan), as previously outlined (32).

Live/dead (AO/PI) staining assay

The Acridine Orange/Propidium Iodide (AO/PI) differential staining assay was employed to assess cell viability following exposure to different nanoformulations. At the specified time points (3, 7, and 14 days) following treatment with HAP, HAP-HYA, and VitC@HAP-HYA to promote OSD, the culture medium was removed, and cells were rinsed twice with 1x PBS. Adherent cells were subsequently detached through incubation with a Trypsin-EDTA solution (250 µl). The cell suspension was collected and centrifuged at 500×g for 3 min to pellet the cells. The supernatant was removed, and the cell pellet was carefully re-suspended in a specified volume of 1x PBS (50 µl). A working solution of the AO/PI stain was prepared immediately before use by diluting stock solutions to a final concentration of 0.4 µg/mL for both AO and PI in 1x PBS. An equal volume of the cell suspension and the AO/PI working solution was mixed

gently (20 µl of cell suspension with 20 µl of stain). The stained cells were incubated in the dark for 5 min at room temperature. A 20 µl aliquot of the mixture was promptly deposited onto a glass slide. Cell viability was evaluated with an Olympus CKX53 fluorescent microscope employing suitable excitation and emission filters. Viable cells were characterized by intact membranes and uniform green nuclear staining due to AO uptake, whereas non-viable or apoptotic cells exhibited compromised membranes and PI uptake, leading to red or orange nuclear staining. Cell counts were conducted across various fields of view (33).

DAPI nuclear staining

The HAP, HAP-HYA, and VitC@HAP-HYA composite biomaterials were sterilized and subsequently positioned in the wells of a 24-well tissue culture plate. MC3T3-E1 pre-osteoblasts were cultured following established laboratory protocols. A 20 µl aliquot of the MC3T3-E1 cell suspension (1×10^5 cells/ml) was directly seeded onto the surface of each composite. The cell-seeded composites were incubated for two hours at 37 ˚C in a humidified atmosphere containing 5% CO_2 to facilitate initial cell adhesion. After the initial adhesion period, unattached cells were eliminated by washing the composites twice with sterile PBS. The adhered cells were subsequently fixed with 4% paraformaldehyde at room temperature. Following fixation, the cell nuclei were stained by incubating the composites with DAPI for 20 min. The adhesion and expansion of MC3T3-E1 cells on the composite surfaces were visualized using an Olympus CX43 fluorescent microscopy platform. Images were obtained from various fields for each sample to evaluate cell coverage and morphology.

Monitoring intracellular ROS

MC3T3-E1 cells were examined for intracellular ROS using immunofluorescence imaging and direct content measurement. MC3T3-E1 cells (1×10^4 cells/well) were grown on coatings in 48-well plates for 24 hr, with or without H_2O_2 treatment, for immunofluorescence. Following a PBS rinse, cells were treated with 10 µM DCFH-DA for 20 min at 37 ˚C, washed, and fixed with 2% paraformaldehyde for 30 min before laser confocal microscopy observation. Similar steps were used to measure intracellular ROS. After 7 and 14 days of incubation, cells were stained with 25 µM DCFH-DA for 45 min at room temperature. After three washes, cells were lysed in 0.3 ml of lysis solution for 10 min at 37 ˚C. A fluorescent enzyme marker evaluated fluorescence intensity at 525 nm when the lysate was transferred to a 96-well plate.

Statistical analysis

Each experiment was conducted in triplicate. The data is presented as the mean with the standard deviation shown as a range. We used GraphPad Prism 8 and one-way ANOVA to determine whether a statistically significant difference existed. At $P<0.05$, the differences were considered statistically significant.

Results

Functional group studies

FT-IR spectroscopy was employed to analyze the functional groups of HAP, HYA, HAP-HYA, and VitC@HAP-HYA (Figure 1a). The HAP spectrum displayed characteristic peaks for phosphate groups at 1090, 960, 600, and 565 cm^{-1}, whereas HYA presented distinct bands corresponding to its carbohydrate and amide components. The HAP-HYA composite exhibited peaks from both components, thereby confirming successful conjugation. Additionally, the emergence of new peaks at 1410 cm^{-1} and 1240 cm^{-1} suggests an interaction between HAP and HYA. The VitC@HAP-HYA spectrum exhibited all peaks from HAP-HYA, in addition to new signals at 1750 cm^{-1} and 1660 cm^{-1}, which correspond to the C=O stretching of the lactone ring and the enol group of VitC, respectively. Minor alterations in the positions of the HAP-HYA peaks in the VitC@HAP-HYA spectrum provided additional confirmation of VitC loading and possible interactions within the composite. A band centered at 3440 cm^{-1} was observed in all samples, indicating overlapping O-H stretching vibrations from hydroxyl groups and adsorbed water. The observed characteristic peak shifts and new

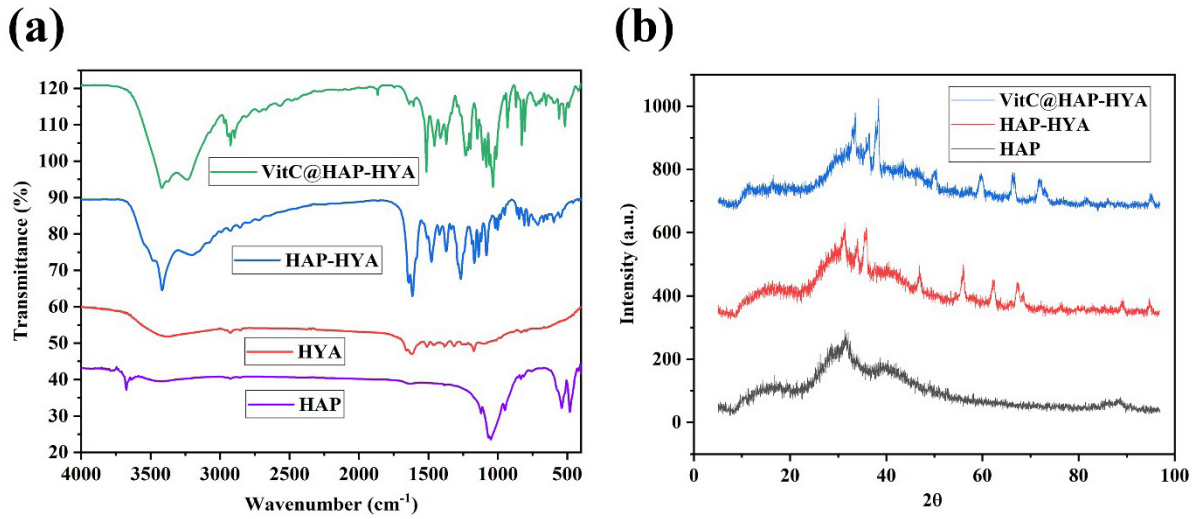

Figure 1. (a) FT-IR analysis of HAP, HYA, HAP-HYA, and VitC@HAP-HYA, showing the characteristic functional groups present in each composite. (b) XRD spectra comparing the crystalline phases of HAP, HAP-HYA, and VitC@HAP-HYA, demonstrating the structural characteristics of each composite
HAP: Hydroxyapatite; HYA: Hyaluronic acid; Vit C: Vitamin C

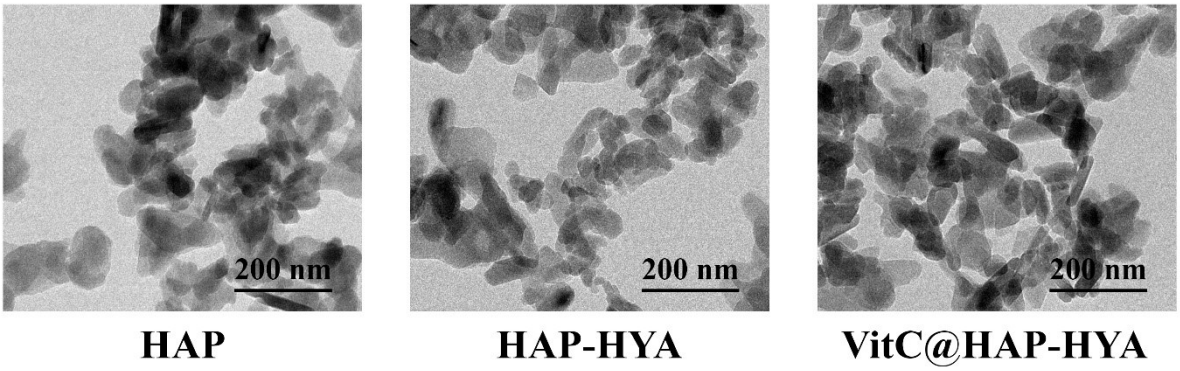

Figure 2. TEM micrographs showing the morphology and ultrastructure of HAP, HYA, HAP-HYA, and VitC@HAP-HYA composites
HAP: Hydroxyapatite; HYA: Hyaluronic acid; Vit C: Vitamin C

bands in HAP-HYA and VitC@HAP-HYA confirm the successful formation of stable nanocomposites via chemical interactions among the components.

Crystalline phase analysis

XRD analysis validated the successful fabrication of the VitC@HAP-HYA nanocomposite (Figure 1b). Both HAP-HYA and the final composite exhibited the characteristic crystalline diffraction peaks of HAP at 2θ≈25.9°, 32.9°, and 39.8°. A slight reduction in peak intensity was observed in both composites compared to pure HAP, indicating that the inclusion of amorphous components (HYA and VitC) affected the bulk crystallinity of HAP. The lack of new diffraction peaks in the VitC@HAP-HYA spectrum suggests that VitC exists in an amorphous or molecularly dispersed form.

Morphological analysis

HR-TEM validated the crystalline structure of the HAP, HAP-HYA, and VitC@HAP-HYA materials (Figure 2). Pure HAP exhibited distinct rod-like particles with prominent lattice fringes, with an average dimension of approximately 50 nm. The HAP-HYA composite exhibited a slight widening of the lattice fringes, as supported by XRD data, suggesting a decrease in HAP crystallinity. Additionally, the particle size increased to approximately 90 nm as a result of HYA incorporation. The VitC@HAP-HYA nanospheres displayed a morphology similar to that of HAP-HYA, with no notable structural alterations, and an increased particle size of approximately 120 nm. The HR-TEM findings, along with XRD data, offer a thorough understanding of the structural and compositional properties of the VitC@HAP-HYA nanoformulation.

The *in vitro* bone regeneration capabilities of the VitC@HAP-HYA scaffold were evaluated utilizing the SBF technique. After 24 hr of incubation in SBF, initial calcium phosphate crystal formation was observed on the scaffold surface. The enhancement of crystal growth and nucleation occurred over a period of three days. After seven days of incubation, a dense and uniform layer of calcium phosphate crystals was observed, as verified by SEM (Figure 3). The rapid formation of apatite in a simulated physiological environment indicates that the VitC@HAP-HYA composite exhibits significant bioactivity and a strong potential to enhance scaffold-guided bone regeneration through the induction of a mineral layer that resembles native bone.

Osteogenic differentiation in MC3T3-E1 on vitC@HAP-HYA

ALP activity, an early biochemical marker for OSD, was measured in MC3T3-E1 cells cultivated on HAP, HAP-HYA, and VitC@HAP-HYA composites at 1, 3, and 7 days into 3, 5, and 7 days. The VitC@HAP-HYA composite had considerably greater and sustained ALP activity than the HAP and HAP-HYA composites in the first week of culture (Figure 4), indicating its better ability to boost early osteogenic commitment. VitC directly stimulates OSD and ALP activity in MC3T3-E1 cells; hence, its synergistic effect within the HAP-HYA matrix may explain this improved

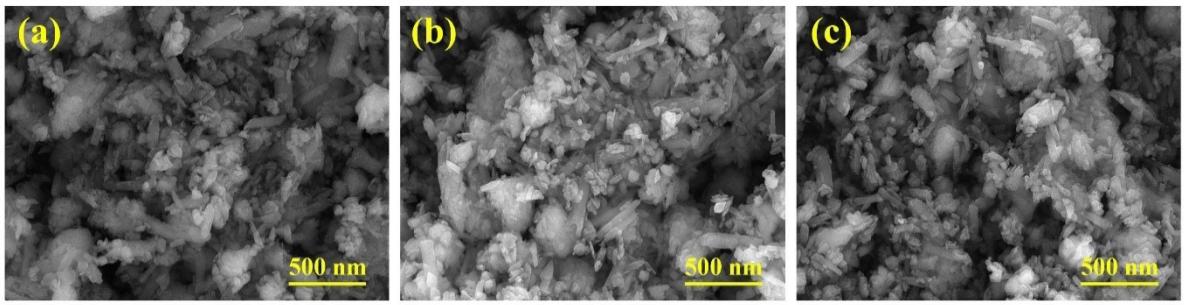

Figure 3. SEM images depicting mineral deposition analysis of the VitC@HAP-HYA composite after incubation in simulated Body Fluid (SBF) solution for (a) 1 day, (b) 3 days, and (c) 7 days
HAP: Hydroxyapatite; HYA: Hyaluronic acid; Vit C: Vitamin C

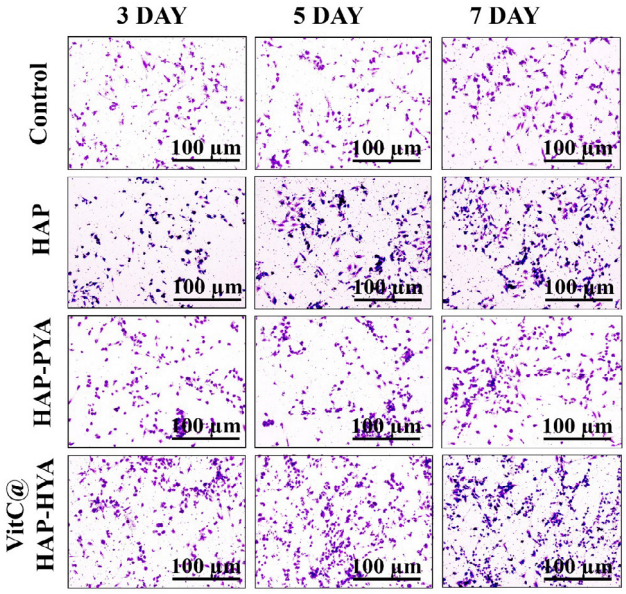

Figure 4. Alkaline phosphatase (ALP) activity of HAP, HAP-HYA, and VitC@HAP-HYA composites
(a) Staining and (b) quantification at 3, 5, and 7 days
HAP: Hydroxyapatite; HYA: Hyaluronic acid; Vit C: Vitamin C

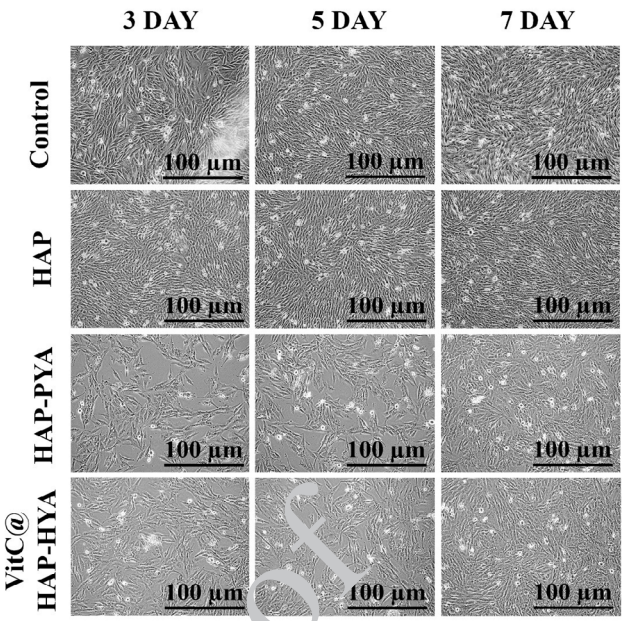

Figure 5. MTT assay results showing the viability of MC3T3-E1 undergoing osteogenic differentiation (ODS) on HAP, HAP-HYA, and Vit C@HAP-HYA composites
(a) Cell viability morphology. (b) Quantification of cell viability at 3, 5, and 7 days
HAP: Hydroxyapatite; HYA: Hyaluronic acid; Vit C: Vitamin C

performance. High early ALP expression implies significant osteogenic pathway activation, showing the VitC@HAP-HYA combination is superior for beginning and developing OSD, showcasing its bone regeneration potential.

Biocompatibility MC3T3-E1cells on vitC@HAP-HYA

The MTT experiment showed that the VitC@HAP-HYA composite increased MC3T3-E1 cell viability over 7 days compared to HAP and HAP-HYA alone, indicating that it promotes cell proliferation and health (Figure 5). The three materials had high cell viability and no time-dependent toxicity. Microscopic study showed that VitC@HAP-HYA-cultured MC3T3-E1 cells had a well-distributed morphology with numerous filopodia, indicating robust cell attachment and spreading. VitC (protecting against oxidative stress and promoting OSD) and HYA (improving cell adhesion and nutrient transport) synergistically improve the VitC@HAP-HYA composite's biocompatibility and cell vitality, making it a promising bone regeneration candidate.

Live/dead MC3T3-E1 cells on vitC@HAP-HYA

All tested scaffolds (HAP, HAP-HYA, and VitC@HAP-HYA composite) demonstrated excellent cytocompatibility with MC3T3-E1 cells across all time points (days 1, 3, and 7 into days 3, 7, and 14), as indicated by prominent green fluorescence from AO staining (live cells) and only intermittent red fluorescence from PI staining (dead cells)(Figure 6). This high cell viability and durability are

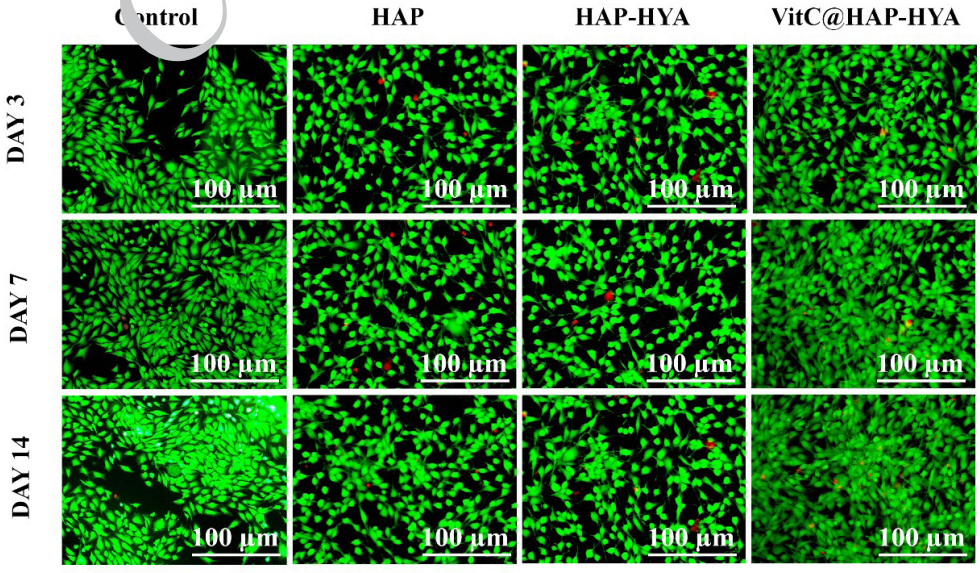

Figure 6. Acridine Orange/Propidium Iodide (AO/PI) live/dead staining of cells cultured on HAP, HAP-HYA, and VitC@HAP-HYA composites, showing cell viability at 1, 3, and 7 days into 3, 7, and 14 day
HAP: Hydroxyapatite; HYA: Hyaluronic acid; Vit C: Vitamin C

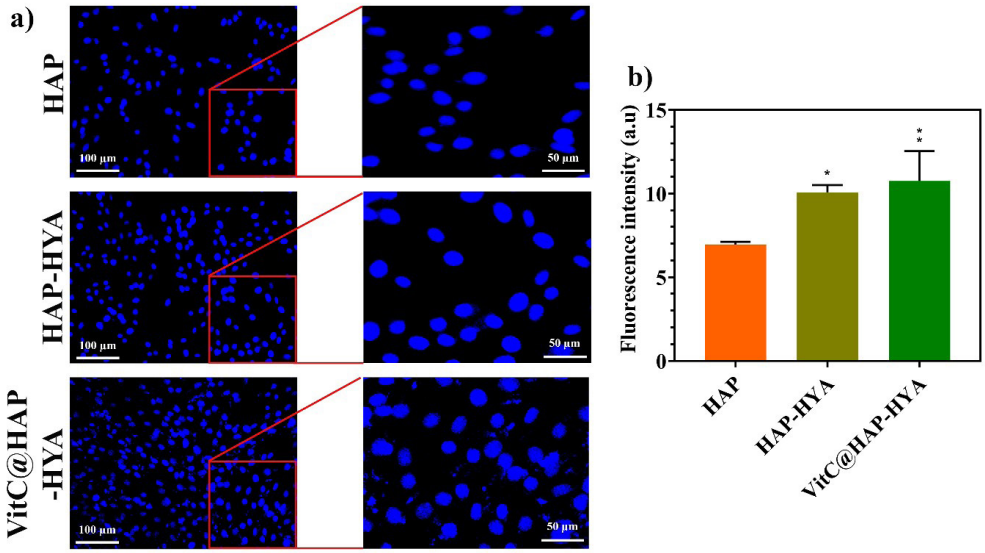

Figure 7. Cellular integration of HAP, HAP-HYA, and VitC@HAP-HYA composite
(a) Visualization of MC3T3-E1 cell adhesion and expansion on the composite surface after 24 hr. (b) Quantitative analysis of DAPI levels in MC3T3-E1 cells cultured on HAP, HAP-HYA, and VitC@HAP-HYA surfaces after 24 hr of treatment
HAP: Hydroxyapatite; HYA: Hyaluronic acid; Vit C: Vitamin C

consistent with the known biomimetic and osteoconductive properties of HAP-based materials and the cell adhesion and proliferation-enhancing effects of HYA. Although the VitC@HAP-HYA composite showed a slight, non-statistically significant reduction in cell viability compared to HAP at later time points, the scaffold remains promising due to the combined advantages of HYA's growth-promoting effects and the continuous release of VitC, which is crucial for collagen synthesis and MC3T3-E1 osteogenic differentiation. Thus, the potential for enhanced osteogenic lineage differentiation is considered a more critical factor for bone regeneration than a minor reduction in initial cell viability.

DAPI staining of vitC@HAP-HYA

The VitC@HAP-HYA composite demonstrated significant potential for cellular integration, an essential feature for BTE applications. MC3T3-E1 cells uniformly colonized the biomaterial surface without morphological changes, as visualized by DAPI nuclear staining (Figure 7). The uniform cellular coverage and lack of altered cell morphology indicate that the VitC@HAP-HYA composite exhibits favorable biocompatibility and bioactivity, aligning with the chemical structural similarity of its HAP component to native bone tissue. The effective colonization of the composite indicates its potential as a scaffold for cellular development and tissue regeneration.

Biomineralization on VitC@HAP-HYA

ARS staining was employed to evaluate the mineralization potential of the VitC@HAP-HYA composite in comparison to HAP and HAP-HYA scaffolds over a period of 21 days into 7 days (Figure 8). Calcium deposition progressed in a time-dependent manner across all groups, with initiation around 10 days into 3 days. On 14 days into 5 days, the intensity of ARS staining increased, with the VitC@HAP-HYA composite exhibiting significantly greater calcium phosphate deposits than either the HAP or HAP-HYA groups. The superior mineralization persisted, with VitC@HAP-HYA demonstrating the highest level of calcium deposition and staining by 21 days into 7 days. The evidence indicates that the VitC@HAP-HYA composite markedly enhances mineralization, likely owing to prolonged VitC release, which is known to increase alkaline phosphatase activity and ECM synthesis. The findings support the potential of the VitC@HAP-HYA composite as a biocompatible and osteogenic scaffold for enhanced bone tissue regeneration.

Cytoprotective vitC@HAP-HYA

The VitC@HAP-HYA composite demonstrates enhanced cytoprotection of osteoblasts under oxidative

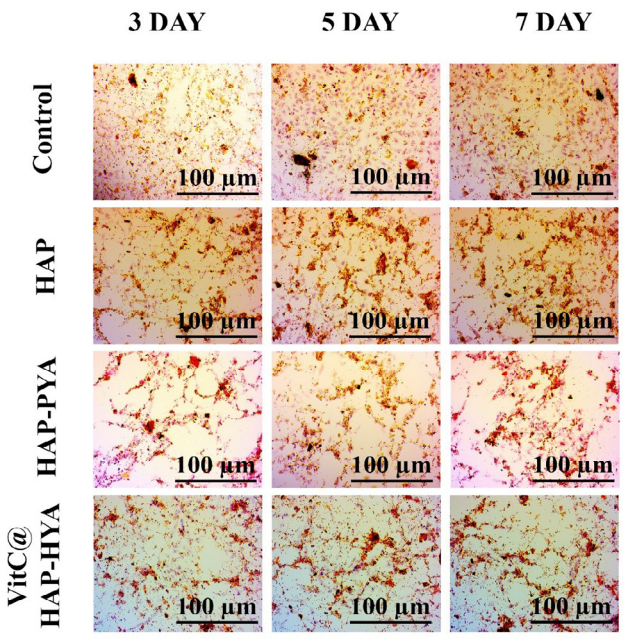

Figure 8. Mineralization assessment of HAP, HAP-HYA, and VitC@HAP-HYA composites by Alizarin Red S (ARS) staining at 10, 14, and 21 days
HAP: Hydroxyapatite; HYA: Hyaluronic acid; Vit C: Vitamin C

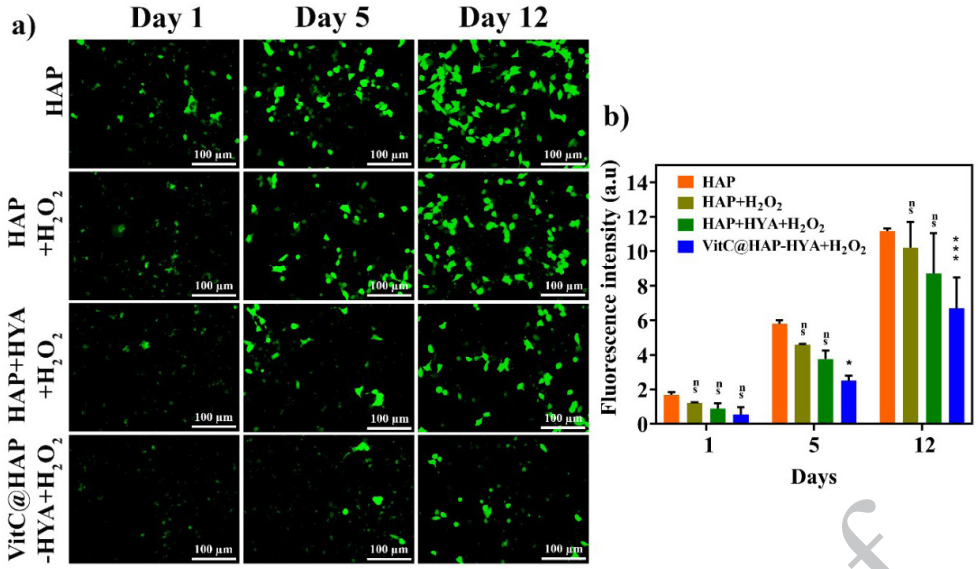

Figure 9. (a) Fluorescence images depicting intracellular reactive oxygen species (ROS) levels in cells cultured on various surfaces (HAP, HAP-HYA, and VitC@HAP-HYA) after 1, 5, and 12 days, as determined by DCFH-DA assay. Cells were either untreated or treated with H_2O_2. (b) Quantitative analysis of intracellular ROS levels in cells cultured on HAP, HAP-HYA, and VitC@HAP-HYA surfaces, with and without H_2O_2 treatment, at days 1, 5, and 12
HAP: Hydroxyapatite; HYA: Hyaluronic acid; Vit C: Vitamin C

stress. Hydrogen peroxide (H_2O_2) suppressed cell growth on control surfaces, but the VitC@HAP-HYA composite markedly promoted cell proliferation, surpassing that of untreated cells on a pure HAP surface (Figure 9 a-b). This effect is attributable to the robust antioxidant properties of the included VitC. The quantitative examination of intracellular ROS revealed that VitC@HAP-HYA markedly inhibited ROS production after H_2O_2 exposure, essentially normalizing ROS levels to those seen under standard culture conditions after 12 days. The results affirm that the VitC@HAP-HYA composite is biocompatible and effectively reduces oxidative stress, indicating its suitability for enhancing osteoblast functionality and osseointegration in adverse physiological conditions marked by oxidative stress.

Discussion

The osteoconductive properties of HAP, the ability of HYA to mimic the ECM, and the osteoinductive potential of VitC were all successfully utilized in the development of the VitC@HAP-HYA nanocomposite. This led to the creation of a promising scaffold for BTE.

The successful conjugation of HAP and HYA was verified by physicochemical characterization using FT-IR, which demonstrated the appearance of new peaks at around 1410 cm^{-1} and 1240 cm^{-1}, confirming the presence of an effective interaction (34). Additionally, the existence of VitC was confirmed by the distinctive C=O stretching (1750 cm^{-1}) and enol group (1660 cm^{-1}) peaks. The HAP-HYA bands exhibited modest shifts, which indicates that the components are in close contact with each other (35, 36). The continuing existence of the crystalline structure of HAP was verified by XRD analysis; nevertheless, there was a significant reduction in the intensity of the peaks in the HAP-HYA and VitC@HAP-HYA composites. This decrease in crystallinity, which corresponds to the broadening of lattice fringes that has been detected in TEM micrographs, indicates that the integration of HYA and the loading of VitC have an impact on the structure of the HAP. This phenomenon is often reported in polymer-inorganic nanocomposites (37). The lack of discrete diffraction peaks for VitC, together with the FT-IR data, provides strong evidence that VitC is scattered in an amorphous or molecularly distributed state inside the composite matrix. The particle size of the pure HAP was approximately 50 nm. This particle size gradually increased to approximately 90 nm in the HAP-HYA and ultimately reached approximately 120 nm in the VitC@HAP-HYA, as shown by the TEM study. This indicates that the integration of HYA and VitC into the HAP framework was effective.

We found that VitC@HAP-HYA performed better in a variety of biological tests. The material's significant *in vitro* bioactivity was validated by SBF analysis, which showed rapid formation of a thick calcium phosphate layer on the scaffold's surface after just 7 days. This suggests a robust potential for apatite synthesis in a physiologically appropriate environment (38). A previous study on the cytocompatibility of HAP-based materials and the cell-adhesion properties of HYA (39, 40) confirmed that all groups exhibited excellent cell viability and proliferation in biocompatibility assays with MC3T3-E1 cells using MTT and AO/PI staining. However, VitC@HAP-HYA demonstrated the best performance. Important components for effective tissue formation include strongly adherent and spreading cells, as evidenced by the evenly dispersed morphology and numerous filopodia of the cells on VitC@HAP-HYA (Figure 5a)(41).

Notably, the combination of VitC@HAP-HYA demonstrated a significant improvement in osteoinductive potential. At every time point, VitC@HAP-HYA exhibited significantly greater early-stage OSD as measured by ALP activity than HAP and HAP-HYA. This consistent increase in ALP activity is a critical marker of enhanced early osteogenic commitment, directly driven by the synergistic action of VitC within the matrix (29, 42). On the same note, the ARS staining showed that VitC@HAP-HYA showed the highest levels of calcium deposition and mineralization on

days 10, 14, and 21 days into 3, 5, and 7 days (Figure 8). VitC enhances biomineralization by accelerating the formation of a robust ECM by stimulating ALP activity, which is necessary for collagen production and cross-linking (43). The use of scaffolds loaded with VitC for improved bone regeneration is strongly supported by these data (44, 45).

In addition, the VitC@HAP-HYA composite effectively shielded cells from oxidative stress. Figure 9 shows that of the cell proliferation decrease and intracellular ROS formation suppression effects of H_2O_2-treated cells, VitC@HAP-HYA had the greatest impact. The capacity of VitC@HAP-HYA to almost restore ROS levels to normal levels under culture conditions highlights its superior cytoprotective mechanism, since ROS-induced oxidative stress is a critical pathogenic component in metabolic bone disorders. Because of VitC's natural antioxidant properties, this discovery has important implications for improving implant osseointegration in difficult physiological settings. Collectively, our findings suggest that the VitC@HAP-HYA composite integrates multiple functions, resulting in a scaffold with enhanced bioactivity, more favorable osteogenic potential, and essential cytoprotective properties. According to current research, VitC@HAP-HYA has the potential to be used in a variety of advanced bone regeneration procedures, including the anti-cancer bone excision approach.

Conclusion

The successful fabrication and characterization of the VitC@HAP-HYA nanocomposite validate the efficient amalgamation of osteoconductive HAP, extracellular matrix-resembling HYA, and osteoinductive VitC into a unified scaffold. Physicochemical investigations, including FT-IR and XRD, substantiated the chemical interactions and the effective incorporation of amorphous or molecularly distributed VitC within the composite. In contrast, HR-TEM corroborated the progressive enlargement of particle size, reaching around 120 nm. Importantly, *in vitro* biological studies indicated that the VitC@HAP-HYA composite markedly surpassed its HAP and HAP-HYA equivalents. It demonstrated rapid apatite production in SBF, displayed exceptional biocompatibility and cell proliferation with MC3T3-E1 cells, and, most importantly, markedly improved early-stage OSD (elevated and sustained alkaline phosphatase activity) and long-term biomineralization (Alizarin Red S staining). Moreover, the composite exhibited a significant cytoprotective effect, significantly inhibiting H_2O_2-induced intracellular ROS production. The results collectively indicate that the VitC@HAP-HYA nanocomposite is a highly promising, multifunctional scaffold with enhanced bioactivity, superior osteogenic potential, and inherent antioxidant properties, making it an exceptional candidate for advanced applications in BTE and regeneration.

Acknowledgment

This project did not receive specific external funding. The authors are grateful for the support and facilities provided by the Department of Chemistry, Rajalakshmi Institute of Technology, Kuthambakkam, Chembarambakkam, Tamil Nadu, India.

Data Availability Statement

The data used to support the findings of this study are available from the corresponding author upon request.

Authors' Contributions

P S contributed to conceptualization, data curation, methodology, validation, visualization, and both the initial and review stages of writing. S R was involved in conceptualization, data curation, visualization, and both drafting and reviewing the manuscript. S S handled data curation, validation, visualization, and both writing phases. R T contributed to conceptualization, data curation, formal analysis, funding acquisition, investigation, methodology, supervision, validation, and both drafting and reviewing. P K participated in conceptualization, data curation, visualization, and both stages of writing. G D contributed to conceptualization, data curation, visualization, and both drafting and reviewing. J K was responsible for data curation, visualization, and review & editing of the manuscript.

Conflicts of Interest

The authors declare no conflicts of interest.

Declaration

We have not used any AI tools or technologies to prepare this manuscript.

References

1. Santoro A, Voto A, Fortini L, Guida R, Laudisio C, Cillo M, D'Ursi AM. Bone defect treatment in regenerative medicine: Exploring natural and synthetic bone substitutes. Int J Mol Sci 2025; 26: 3085-3101.
2. Khobragade SS, Deshmukh M, Vyas U, Ingle RG. Innovative approaches in bone tissue engineering: Strategies for cancer treatment and recovery. Int J Mol Sci 2025; 26: 3937-3958.
3. Haghighat M, Gharavian M, Azimi E, Tavalaei KN, Akbari Toosi SH, Mohammadi M. Novel bone graft substitutes in bone tissue engineering. Nanomed J 2025; 12: 354-369.
4. Cota Quintero JL, Ramos-Payán R, Romero-Quintana JG, Ayala-Ham A, Bermúdez M, Aguilar-Medina EM. Hydrogel-based scaffolds: Advancing bone regeneration through tissue engineering. Gels 2025; 11: 175-213.
5. Ivanova N, Ivanov S, Peev S, Dikova T. Types of bone substitutes and their application in regenerative medicine: A systematic review. J Funct Biomater 2025; 16: 341-389.
6. Abushama AA, Alim N, AlTuraiki AM, AlQahtani TT, Alotaibi NT, AlQahtani MM, *et al.* Comparison of xenograft and allograft bone graft for oral and maxillofacial surgical preparation prior to dental implantation: A systematic review. F1000Res 2025; 14: 718-732.
7. Kim YW, Cosola S, Kim YS, Park YM, Covani U, Fabbri A, Menchini-Fabris GB. Clinical application of rhBMP-2 and three-dimensinal preformed titanium mesh with allograft and xenograft for peri-implant horizontal and vertical bone augmentation–a narrative review with technical report. J Clin Med 2025; 14: 4788-4809.
8. Hosseini R, Rashidi J, Mokhtariyan M, Landarani-Isfahani A. Fabrication and morphology of biomaterials based on the used synthesis methods. In Green Biomaterials in Tissue Engineering 2025. pp. 89-140. American Chemical Society.
9. Tarwate Y, Khandke A, Kulkarni M, Banode K, Patel M, Pardeshi K, Rajput A. Biomaterials-based additive manufactured products for *in situ* tissue engineering. In Biomaterial-based Additive Manufacturing in Tissue Engineering and Regeneration Cham: Springer Nature Switzerland. 2025. pp. 313-371.
10. Dixon DT, Gomillion CT. Conductive scaffolds for bone tissue engineering: Current state and future outlook. J Funct Biomater 2021; 13: 1-24.
11. Sharma S, Sudhakara P, Singh J, Ilyas RA, Asyraf MR, Razman MR. Critical review of biodegradable and bioactive polymer composites for bone tissue engineering and drug delivery

applications. Polymers 2021; 13: 2623-2688.
12. Misra SK, Boccaccini AR. Biodegradable and Bioactive Polymer/ceramic Composite Scaffolds. In Tissue engineering using ceramics and polymers. Woodhead Publishing. 2007. pp. 72-92.
13. Govindaraj D, Rajan M, Munusamy MA, Alarfaj AA, Sadasivuni KK, Kumar SS. The synthesis, characterization and *in vivo* study of mineral substituted hydroxyapatite for prospective bone tissue rejuvenation applications. Nanomedicine 2017; 13: 2661-2669.
14. Govindaraj D, Rajan M, Munusamy MA, Higuchi A. Mineral substituted hydroxyapatite coatings deposited on nanoporous TiO_2 modulate the directional growth and activity of osteoblastic cells. RSC Adv 2015; 5: 58980-58988.
15. Bhat S, Uthappa UT, Altalhi T, Jung HY, Kurkuri MD. Functionalized porous hydroxyapatite scaffolds for tissue engineering applications: A focused review. ACS Biomater Sci Eng 2021; 8: 4039-4076.
16. George SM, Nayak C, Singh I, Balani K. Multifunctional hydroxyapatite composites for orthopedic applications: A review. ACS Biomater Sci Eng 2022; 8: 3162-3186.
17. Rooney P, Kumar S. Inverse relationship between hyaluronan and collagens in development and angiogenesis. Differentiation 1993; 54: 1-9.
18. Ye H, Zhang R, Zhang C, Xia Y, Jin L. Advances in hyaluronic acid: Bioactivity, complexed biomaterials and biological application: A review. Asian J Surg 2025; 48: 49-61.
19. Yue S, He H, Li B, Hou T. Hydrogel as a biomaterial for bone tissue engineering: A review. Nanomaterials 2020; 10: 1511-1535.
20. Sumathra M, Govindaraj D, Jeyaraj M, Al Arfaj A, Munusamy MA, Kumar SS, *et al.* Sustainable pectin fascinating hydroxyapatite nanocomposite scaffolds to enhance tissue regeneration. Sustain Chem Pharm 2017; 5: 46-53.
21. Patra P, Upadhyay TK, Alshammari N, Saeed M, Kesari KK. Alginate-Chitosan biodegradable and biocompatible based hydrogel for breast cancer immunotherapy and diagnosis: A comprehensive review. ACS Appl Bio Mater 2024; 7: 3515-3534.
22. Dethlefs-Canto J, Osses-Barría F, Vergara-Zenteno R, Bust[illegible]-Ponce A, Villavicencio-Duarte J. The effectiveness of vitamin C in dental alveolus healing after dental extraction: A scoping review. Med Oral, Patol Oral Cir Bucal 2024; 30: e124-128.
23. Zhang J, Zhang Q, Lin G, Wang Y, Li J, Wang P, *et al.* Single-cell analysis reveals that vitamin C inhibits bone metastasis of renal cancer via cell cycle arrest and microenvironment remodeling. Adv Sci 2025; 12: e01011-01027.
24. Ambrosio L, Cecchini A, Pellacani G, Cesforo C. Exploratory evaluation of a hyper-diluted calcium hydroxyapatite–hyaluronic acid combination for facial rejuvenation: A pilot study. Cosmetics 2025; 12: 212-224.
25. Kasi PB, Serafin A, O'Br[illegible] L, Moghbel N, Novikov LN, Kelk P, Collins MN. Electroconductive gelatin/hyaluronic acid/hydroxyapatite scaffolds for enhanced cell proliferation and osteogenic differentiation in bone tissue engineering. Biomater Adv 2025;173: 214286-214303.
26. Gerk SA, Nashchekinab YA, Golovanova OA. Study of resorption and cytotoxicity of composites based on carbonate hydroxyapatite and high molecular weight hyaluronic acid *in vitro*. J Siberian Federal Univ Chemi 2025; 18: 64-73.
27. Xu Y, Qi J, Sun W, Zhong W, Wu H. Corrigendum: Therapeutic effects of zoledronic acid-loaded hyaluronic acid/polyethylene glycol/nano-hydroxyapatite nanoparticles on osteosarcoma. Front Bioeng Biotechnol 2025; 13: 1601751-1601753.
28. Kianfar R, Kanani R, Janmohammadi H, Olyaee M, Besharati M, Lackner M. Implications of high-dose vitamin D3 with and without vitamin C on bone mineralization and blood biochemical factors in broiler breeder hens and their offspring. PeerJ 2025; 13: e18983-19002.
29. Majumdar U, Bose S. Curcumin and vitamin C dual release from Hydroxyapatite coated Ti6Al4V discs enhances *in vitro* biological properties. Mater Chem Phys 2024; 313: 128622-128644.
30. Dong W, Matsukawa Y, Long Y, Hayashi Y, Nakamura J, Suzuki K, Ohtsuki C. Revised method for preparation of simulated body fluid for assessment of the apatite-forming ability of bioactive materials: proposal of mixing two stock solutions. RSC Adv 2024; 14: 38660-38667.
31. Kaliannagounder VK, Hossain MA, Kim JH, Thangavelu M, Adithan A. Magnetic hydroxyapatite composite nanoparticles for augmented differentiation of MC3T3-E1 cells for bone tissue engineering. Mar Drugs 2023; 21: 85-100.
32. Oh YW, Kang SW, Park S, Park SW, Yi HG. Collagen/hydroxyapatite hydrogels promote intercellular interactions and osteogenic differentiation. J Biomed Mater Res B Appl Biomater 2025; 113: e35632-35643.
33. Munusamy S, Karthikeyan P, Kaliamoorthy S, Vadivel P. Biomimetic chitosan/alginate with zinc and strontium hydroxyapatite for periodontal regeneration application. Nanomed J 2025; 12: 1-13.
34. Tan Y, Ma L, Chen X, Ran Y, Tong Q, Tang L, Li X. Injectable hyaluronic acid/hydroxyapatite composite hydrogels as cell carriers for bone repair. Int J Biol Macromol 2022; 216: 547-557.
35. Svarca A, Grava A, Dub[illegible] A, Kamata-Stunda A, Narnickis R, Aunina K, *et al.* Calcium phosphate/hyaluronic acid composite hydrogels for local antitetanotic drug delivery. Front Bioeng Biotechnol 2022; 10: 917765-917786.
36. Hachinohe Y, Tan[illegible] M, Hoshi M, Yoshida D, Hatakeyama W, Sawada T, *et al.* Self-prepared hyaluronic acid/alkaline gelatin composite with nano-hydroxyapatite and bone morphogenetic protein for cranial bone formation. Int J Mol Sci 2023; 24: 1104-1126.
37. [illegible]ng B, Li Q, Yu B, Zhang J, Yang S, Lu R, *et al.* Dual nanofillers reinforced polymer-inorganic nanocomposite film with enhanced mechanical properties. Small 2024; 20: 2406160.
38. Elmofty AR, Abdel Aziz ME, Tash M, El-Hadad S. Development and characterization of hydroxyapatite and multiwall carbon nanotubes reinforced polypropylene biocomposites. Sci Rep 2025; 15: 18754-18769.
39. Apăvăloaiei I, Nacu I, Cojocaru FD, Balan V, Bercea M, Niță LE, *et al.* Effect of chitosan on 3D printed scaffolds with gelatin–hyaluronic acid, hydroxyapatite and magnetic nanoparticles for bone tissues defects repair. React Funct Polym 2025; 216: 106422.
40. Khodami Moghari N, Asefnejad A. Effect of manufacturing angle on surface characteristics and fibroblast adhesion of polycaprolactone/hyaluronic acid scaffold for tissue engineering. Nanomed J 2025; 12: 768-788.
41. Amiryaghoubi N, Esfahlan RJ. Applications of hydroxyapatite-based polymeric scaffolds in bone tissue engineering: An update. Adv Pharm Bull 2024; 14: 794-806.
42. Zhao B, He J, Wang F, Xing R, Sun B, Zhou Y. Polyacrylamide-sodium alginate hydrogel releasing oxygen and vitamin C promotes bone regeneration in rat skull defects. Front Mater 2021; 8: 758599-758610.
43. Carvalho MS, Cabral JM, da Silva CL, Vashishth D. Bone matrix non-collagenous proteins in tissue engineering: Creating new bone by mimicking the extracellular matrix. Polymers 2021; 13: 1095-1128.
44. Abdulhameed EA, Rani KA, AlGhalban FM, Abou Neel EA, Khalifa N, Khalil KA, *et al.* Managing oxidative stress using vitamin C to improve biocompatibility of polycaprolactone for bone regeneration *in vitro*. ACS Omega 2024; 9: 31776-31788.
45. Hashemi SF, Mehrabi M, Ehterami A, Gharravi AM, Bitaraf FS, Salehi M. *In-vitro* and *in-vivo* studies of PLA/PCL/gelatin composite scaffold containing ascorbic acid for bone regeneration. J Drug Deliv Sci Technol 2021; 61: 102077.